

Increased precipitation weakenes the positive effect of vegetation greening on erosion

Xuling Luo, Xiaoyong Bai, Chaoyong Shen, Ruidong Yang, Yue Cao, Luhua Wu, Fei Chen, Chen Ran, Min Liu & Yu Zhang

To cite this article: Xuling Luo, Xiaoyong Bai, Chaoyong Shen, Ruidong Yang, Yue Cao, Luhua Wu, Fei Chen, Chen Ran, Min Liu & Yu Zhang (2023) Increased precipitation weakenes the positive effect of vegetation greening on erosion, Geocarto International, ahead-of-print:ahead-of-print, 2172216, DOI: [10.1080/10106049.2023.2172216](https://doi.org/10.1080/10106049.2023.2172216)

To link to this article: <https://doi.org/10.1080/10106049.2023.2172216>



© 2023 The Author(s). Published by Informa UK Limited, trading as Taylor & Francis Group



View supplementary material [↗](#)



Published online: 29 Jan 2023.



Submit your article to this journal [↗](#)



Article views: 751



View related articles [↗](#)



View Crossmark data [↗](#)



Increased precipitation weakens the positive effect of vegetation greening on erosion

Xuling Luo^{a,b,c}, Xiaoyong Bai^{a,b,d,e} , Chaoyong Shen^{a,c,f}, Ruidong Yang^a, Yue Cao^b, Luhua Wu^b, Fei Chen^b, Chen Ran^b, Min Liu^b and Yu Zhang^a

^aCollege of Resources and Environmental Engineering, Guizhou University, Guiyang, Guizhou, China;

^bState Key Laboratory of Environmental Geochemistry, Institute of Geochemistry, Chinese Academy of Sciences, Guiyang, Guizhou Province, China; ^cThe Third Surveying and Mapping Institute of Guizhou Province, Guiyang, China; ^dCAS Center for Excellence in Quaternary Science and Global Change, Xi'an, Shanxi Province, China; ^eGuizhou Provincial Key Laboratory of Geographic State Monitoring of Watershed, Guizhou Education University, Guiyang, China; ^fGuizhou Academy of Sciences, Guiyang, China

ABSTRACT

Soil erosion is a major global soil degradation problem that threatens land, freshwater and oceans. Rainfall erosivity has led to an increasing in the global soil erosion rate, while vegetation restoration is a safeguard measure to reduce soil erosion. Therefore, probing the influence of precipitation and vegetation on the spatial distribution of soil erosion is important for understanding the mechanism of erosion. In order to assess the degree of global soil erosion, based on the RUSLE model, a global soil erosion data set from 2000 to 2015 ($0.25^{\circ} \times 0.25^{\circ}$) was created, showing that soil erosion was increasing in 70.80% of the study area, where precipitation was the dominant factor. Different grades of erosion showed that the soil erosion area of mild and above mild erosion increased by 44.88×10^6 ha, an increase of 5.39%. Spatial erosion is mainly distributed in Asia and North America. The difference from North America is that the erosion in Asia showed a decreasing trend during the study period. Different climatic zones show that erosion mainly occurs in the temperate zone, accounting for 39.97% of the area. Precipitation and vegetation increasing significantly in 24.43% and 16.74% of the regions. However, the proportion of regions where precipitation and vegetation had a negative contribution to erosion was 29.12% and 53.81%. Above results will deepen our understanding of the mechanism of erosion.

ARTICLE HISTORY

Received 2 August 2022
Accepted 18 January 2023


KEYWORDS

Climate change; soil erosion; global change; spatial distribution

1. Introduction

Soil erosion is a major global soil degradation problem that threatens land, freshwater and oceans (Borrelli et al. 2020), and a major threat to food security and ecosystem

CONTACT Xiaoyong Bai  baixiaoyong@vip.skleg.cn

 Supplemental data for this article can be accessed online at <https://doi.org/10.1080/10106049.2023.2172216>.

© 2023 The Author(s). Published by Informa UK Limited, trading as Taylor & Francis Group

This is an Open Access article distributed under the terms of the Creative Commons Attribution License (<http://creativecommons.org/licenses/by/4.0/>), which permits unrestricted use, distribution, and reproduction in any medium, provided the original work is properly cited.

viability (David and Michael 2013; Robinson et al. 2017; Wuepper et al. 2020), and its impact is widespread, the damage is long-term (Pimentel et al. 1995; Pimentel and Kounang 1998). Every year, about 75 billion tons of soil are eroded in the world's terrestrial ecosystem (Lal 1990; Wen 1998; Williams, 1990). Since soil formation is very slow that the rate of soil loss is 40 times that of soil regeneration and sustainability (Pimentel and Kounang 1998). The United Nations report on the state of global soil resources emphasizes that the state of most soil resources in the world is only average, poor or very poor, and emphasizes that soil erosion is still a major threat to the world's environment and agriculture.

The loss of soil from land surfaces by erosion is widespread globally and adversely affects the productivity of all natural ecosystems as well as agricultural, forest, and rangeland ecosystems (Lal and Stewart 1990). Land area globally affected by erosion is 1094 million ha (M ha) by water erosion, of which 751 M ha is severely affected, and 549 M ha by wind erosion, of which 296 M ha is severely affected (Lal 2003). Increasing soil erosion and phosphorus loss restrict future food and feed production (Van Oost et al. 2007; Alewell et al. 2020). The changes inflicted on soils by human-induced erosion over many years are significant and have resulted in valuable land becoming unproductive and often eventually abandoned (Pimentel et al. 1995). New research shows that approximately 2.8 tons of soil is lost per hectare per year (Borrelli et al. 2017).

Soil erosion is a basic phenomenon that controls the migration and redistribution of soil and related basic elements (such as carbon) in the landscape. It not only affects the distribution of organic carbon, (Liu et al. 2021), but also affects the global carbon cycle (Lal 2003; Zhang et al. 2022; Luo et al. 2022; Bai et al. 2023). Erosion-induced carbon feedback has been studied on the scale of hillsides and small watersheds (Doetterl et al. 2016), and even globally (Wang et al. 2017). People's have further understood of the role of artificially accelerated soil erosion on the biogeochemical cycle of the earth's carbon (Chappell et al. 2016; Lugato et al. 2018). Soil erosion is a complex process that depends on the nature of the soil, the long slope of the ground slope, vegetation, precipitation, and land use changes (Hamilton and Selby 1982). Changes in land use are widely recognized as capable of greatly accelerating soil erosion (Chappell et al. 2011; Chappell et al. 2012). The elevation control, aspect, and drainage network are identified as the major drivers of the distribution of vegetation cover on the landscapes (Srivastava et al. 2022). Therefore, the paper mainly discusses and analyzes the impact of vegetation and precipitation on erosion.

Vegetation and precipitation exert competing effects, precipitation increases and vegetation inhibits erosion (Langbein and Schumm 1958). When the soil lacks protective vegetation cover, it cannot inhibit the runoff caused by precipitation, the rapid runoff by precipitation reduce the water holding capacity of the soil and reduce the soil organic matter, leading to the reduction of nutrients (Yang et al. 2003; Borrelli et al. 2017). From a global perspective, vegetation is increasing (Chen et al. 2019; Yang et al. 2019; Xiao et al. 2022), which includes vegetation greening promoted by ecological engineering (Tong et al. 2018). Although some people currently think that the impact of vegetation restoration on the ecosystem in arid and semi-arid areas is not always positive (Cao et al. 2010; Cao et al. 2011; Schlaepfer et al. 2017). there are still many studies that have reported that vegetation greening can partially offset the increased rainfall stress (Liu et al. 2019), vegetation restoration can enhance soil retention (Wu et al. 2020; Liu et al. 2021). Furthermore, sediment concentration in runoff is shown to increase with decreased annual precipitation, a decrease in precipitation will cause stream channel aggradation (Langbein and Schumm 1958). Vegetation restoration can reduce surface runoff and

sediment transport (Pizarro et al. 2000; FeNG et al. 2012), reduce river flow and reduce soil loss. Consequently, vegetation and precipitation plays a key role in modulating geomorphic processes (Saco & Moreno-de las Heras 2013).

Therefore, the main objectives of this study are to: (1) Analyze the spatial distribution characteristics of soil erosion on the continent and climate zone; (2) Analyze the change trend of soil erosion, and clarify the proportion of the area with increased soil erosion during the study period; (3) Discussed the impact of rainfall and vegetation on erosion. It is hoped that the research on the influence of precipitation and vegetation on erosion can improve our understanding of the driving factors of soil erosion.

2. Materials and methods

2.1. Materials

2.1.1. NDVI data

GIMMS NDVI data comes from the National Oceanic and Atmospheric Administration (<https://www.noaa.gov/>) at a spatial resolution of 8km × 8km over the period 1981-2015. GIMMS NDVI is currently a global continuous dataset with the longest coverage period. In the process of data set preparation, it considers the influence of various factors on NDVI, and goes through a series of processing such as radiometric correction, geometric correction and cloud removal. Furthermore, the effects of volcanic eruption, solar altitude Angle and sensor sensitivity change with time are eliminated. Compared with other NDVI values, GIMMS NDVI can better ensure the data quality and has been widely used in the study of global and regional large-scale vegetation activity changes (Slayback et al. 2003; Kaufmann et al. 2002; Zhu et al. 2016). After obtaining GIMMS NDVI data, we used ENVI software to rotate the original product by 180°. WGS_1984 geographic coordinates are used and converted to Geotiff format. IDL programming language was used to realize image batch cutting and pixel brightness value conversion to NDVI. In the process of data processing, this paper adopts the maximum synthesis method (MVC) to further eliminate the influence of outliers such as clouds and atmosphere. The processed NDVI data are mainly used for estimating vegetation cover management factors and partial correlation analysis.

2.1.2. Precipitation data

The precipitation data comes from the National Centers for Environmental Information (NCEI) (<https://www.ncei.noaa.gov/data/>) of the National Oceanic and Atmospheric Administration (NOAA) (<ftp://ftp.ncdc.noaa.gov/pub/data/noaa/>). According to the website provided, find the 'isd-history' file in the directory, which provides 29726 meteorological stations, including site ID, site latitude and longitude, site elevation, site city, site country, site data start and end time. GHCND Monthly summary database data is derived from GHCN-Daily database, which is made by quality review and secondary processing. It mainly contains 18 meteorological elements, including temperature (monthly average and extreme value), precipitation (monthly total, extreme value and the number of days meeting various quantity thresholds), snow, and maximum snow depth, etc. The GHCND Monthly summary database, like its daily counterpart, contains dozens of observations from more than 40,000 sites spread across continents. The processed monthly scale rainfall data are prepared for later rainfall erosivity estimation.

2.1.3. DEM data

The DEM data was obtained from the Scripps Institute of Oceanography, University of California, San Diego (https://topex.ucsd.edu/www_html/srtm15_plus.html).

Tozer et al. (2019) have created a new global elevation grid, using a spatial sampling interval of 15 arc sec. The spatial resolution is equal to the sampling interval on land and when ocean grid cells are constrained by shipboard soundings, while it is ~ 6 km (half wavelength) for cells constrained by satellite-derived predicted depths. Altimetrically derived depths have RMS uncertainties of ± 150 m in the deep oceans and ± 180 m between coastlines and the continental rise. Topographic data are used to prepare for estimating slope and slope length (LS).

2.1.4. Land use data

Land use comes from the European Space Agency's Climate Change Initiative data set (<https://www.esa-landcover-cci.org/>), and its products are widely used in vegetation function type distribution research (Hartley et al. 2017), product comparison (Shen et al. 2016), model construction (Poulter et al. 2015). The CCI-LC project delivers consistent global LC maps at 300 m spatial resolution on an annual basis from 1992 to 2015. The Coordinate Reference System used for the global land cover database is a geographic coordinate system (GCS) based on the World Geodetic System 84 (WGS84) reference ellipsoid. A key aspect of the CCI-LC maps consists in their consistency over time. As a result, the set of annual maps are not produced independently but they are derived from a unique baseline LC map which is generated thanks to the entire MERIS FR and RR archive from 2003 to 2012. Independently from this baseline, LC changes are detected at 1 km based on the AVHRR time series between 1992 to 1999, SPOT-VGT time series between 1999 and 2013 and PROBA-V data for years 2013, 2014 and 2015. When MERIS FR or PROBA-V time series are available, changes detected at 1 km are re-apped at 300 m. The last step consists in back- and up-dating the 10-year baseline LC map to produce the 24 annual LC maps from 1992 to 2015. That more can be found in the website (http://maps.elie.ucl.ac.be/CCI/viewer/download/ESACCI-LC-Ph2-PUGv2_2.0.pdf).

2.1.5. Soil properties data

Soil properties from the Global Soil Database (HWSD) (<https://www.fao.org/soils-portal/soil-survey/soil-maps-and-databases/harmonized-world-soil-database-v12/en/>) (FAO, 2012). The HWSD is a 30 arc-second raster database with over 16000 different soil mapping units that combines existing regional and national updates of soil information worldwide (SOTER, ESD, Soil Map of China, WISE) with the information contained within the 1:5 000 000 scale FAO-UNESCO Soil Map of the World (FAO, 1971-1981). The resulting raster database consists of 21600 rows and 43200 columns, which are linked to harmonized soil property data. The use of a standardized structure allows for the linkage of the attribute data with the raster map to display or query the composition in terms of soil units and the characterization of selected soil parameters (organic Carbon, pH, water storage capacity, soil depth, cation exchange capacity of the soil and the clay fraction, total exchangeable nutrients, lime and gypsum contents, sodium exchange percentage, salinity, textural class and granulometry) (Fischer et al. 2008). Data preprocessing: find and download 'Database (.mdb) and HWSD Raster' from the above webpage. HWSD Raster was loaded in ARCGIS, then linked with Database (.mdb) and pulled out soil organic matter, clay, sand and. Preparation for calculation of soil erodibility.

2.1.6. Climate type data

The climate type used in this study is Köppen-Geiger climate classification data from the Global Precipitation Climate Center (GPCC) German Meteorological Agency (<http://gpcc.dwd.de>). The climate classification originally proposed by Wladimir Köppen in 1900 and modified by his collaborators and successors is still widely used, and it is widely used in the teaching of climate courses in schools and universities. In addition, researchers in many disciplines still often use it as a basis for variable climate regionalization and evaluation of the output of global climate models (Peel et al. 2007). Therefore, this study draws on the research of predecessors (Yang et al. 2019; Ran et al. 2020) into five categories (Table 1). This data is mainly used to analyze the spatial distribution of soil erosion.

2.2. Methods

2.2.1. RUSLE model

The RUSLE model is currently the most widely used classic model for soil erosion research in the world. It was originally proposed by Wischmeier and Smith in 1958 (Wischmeier and Smith 1958). It can predict soil loss caused by surface erosion and gully erosion. It was approved by the United States Department of Agriculture. The revised general soil loss equation has been applied in 109 countries (Alewell et al. 2019). The equation is expressed as follows:

$$A = R \times K \times L \times S \times C \times P \quad (1)$$

where R is the rainfall erosivity factor; L is the slope length factor, S is the slope factor; K

Table 1. Climatic division.

Climate type	Acronyms	Full name
Tropical climates	Af	Tropical rainforest climate
	Am	Tropical monsoon climate
	Aw	Tropical savanna climate
Arid climates	Bsh	Savanna climate
	Bsk	Temperate steppe climate
	Bwh	Tropical desert climate
	Bwk	Temperate desert climate
Warm temperate climates	Cfa	Summer hot normally humid and warm climate
	Cfb	Warm summer, normal humidity and warm climate
	Cfc	Cool summer/temperate oceanic climate
	Csa	Mediterranean climate with hot summers
	Csb	Warm Mediterranean climate in summer
	Cwa	Hot summer/subtropical monsoon humid climate
	Cwb	Warm summer climate
	Cwc	Cool summer climate
	Cold temperate climates	Dfa
Dfb		Warm summer climate with normal humidity and cold temperature
Dfc		Cool summer climate with normal humidity and cold temperature
Dfd		Significantly continental normal humidity and cold temperature climate
Dsa		Hot and humid continental climate in summer
Dsb		Warm and humid continental climate in summer
Dsc		Subarctic climate
Dsd		Extremely cold subarctic climate
Dwa		Hot summer, dry winter and cold temperature climate
Dwb		Warm summer, dry winter and cold temperature climate
Dwc		Cool in summer, dry and cold in winter
Dwd		Significantly continental climate with dry and cold temperature in winter
Polar climates		ET
	EF	Frost climate

is the soil erodibility factor; C is the land cover and management factor; P is the water and soil conservation measure factor.

2.2.1.1. Rainfall erosivity factor. Rainfall erosivity is the potential ability of rainfall to cause erosion. It is the primary basic factor in the soil loss equation. This factor is related to rainfall, rainfall duration, and rainfall kinetic energy, and can reflect the impact of rainfall characteristics on soil erosion. Since the direct measurement of rainfall erosivity is difficult, most researchers use rainfall parameters to express it. Therefore, based on the monthly data, the following formula is used to calculate the erosivity:

$$R_m = b_0 \times [p_m \times (f(m) + f(E, F))]^{b_1} \quad (2)$$

where p_m is the average monthly rainfall (mm month^{-1}), b_0 and b_1 are empirical coefficients, with values of 0.207 and 1.561 respectively, $f(m)$ is the sine of the month, $f(E, F)$ is a parabolic function reflecting the influence of elevation (E, m) and latitude ($F, ^\circ$) on rainfall erosivity (Diodato and Bellocchi 2007)

$$f(m) = a \times \left[1 - b \cos \left(2\pi \times \frac{m}{c + m} \right) \right] \quad (3)$$

where, m is the monthly value (the value range is 1-12), a, b and c are the empirical coefficients, with the values of 0.3696, 1.0888 and 2.9048 respectively (Hashim GM and Yu B. 2001; Davison P and Hutchins MG, 2005) .

$$f(E, F) = d + e \times \sqrt{E} \times (L_c - L) + g \times \left[\sqrt{E} \times (L_c - L) \right]^2 \quad (4)$$

where E (m) is the elevation value, L ($^\circ$) is the latitude value, L_c ($^\circ$) is the critical latitude, and the value is 41° in this study. d, e and g are the empirical coefficients, with the values of 0.3024, 1.3848E-03 and $-1.38092\text{E-}05$, respectively.

2.2.1.2. Soil erodibility factor. Soil erodibility is an important indicator that reflects the soil's ability to infiltrate rainfall and its sensitivity to rainfall and runoff denudation and transportation, and it is an important internal factor affecting soil loss. The soil erodibility factor (K) is a quantitative value obtained through experiments. It is usually obtained by the amount of soil loss caused by the erosivity of precipitation per unit of standard plots, but it is difficult to achieve large-scale deployment of natural plots around the world. Therefore, this study uses the calculation method of soil erodibility factor developed by Williams (1990) in the EPIC model. The equation expression is as follows:

$$k = 0.1317 \times \left\{ 0.2 + 0.3 \times \exp \left[-0.0256 S_a \times \left(1 - \frac{S_i}{100} \right) \right] \right\} \times \left(\frac{S_i}{S_i + C_l} \right)^{0.3} \\ \times \left[1 - \frac{0.25 \times O_r c}{O_r c + \exp(3.72 - 2.95 O_r c)} \right] \times \left[1 - \frac{0.75 \times S_n}{S_n + \exp(-5.51 + 22.9 \times S_n)} \right] \quad (5)$$

where k is the soil erodibility value. $S_n = 1 - (S_a/100)$, S_a is sand, S_i is silt, C_l is clay, and $O_r c$ is organic matter content (%).

2.2.1.3. Slope and slope length factor. Slope factor and slope length factor are the most important topographical factors affecting soil erosion. For accurate slope and slope length, it requires professionals to conduct field surveys, which is time-consuming and labor-intensive. This method is suitable for large-scale research areas like the world. With the

development of GIS technology, the current slope and slope length are mainly obtained through DEM data. This article draws on the calculation method of slope and length factor of Liu et al. (1994), the equation is expressed as follows:

$$S = \begin{cases} 10.8\sin \theta + 0.03 & (\theta < 5^\circ) \\ 16.8\sin \theta - 0.50 & (5^\circ \leq \theta < 10^\circ) \\ 21.9\sin \theta - 0.96 & (10^\circ \leq \theta) \end{cases} \quad (6)$$

$$L = \left(\frac{\lambda}{22.13} \right)^m \quad (7)$$

$$m = \begin{cases} 0.2 & (\theta \leq 1^\circ) \\ 0.3 & (1^\circ < \theta \leq 3^\circ) \\ 0.4 & (3^\circ < \theta \leq 5^\circ) \\ 0.5 & (5^\circ < \theta) \end{cases} \quad (8)$$

$$\lambda = \text{flowacc} \times \text{cell size} \quad (9)$$

where S is the slope factor, θ is the slope ($^\circ$); L is the slope length factor: flowacc is the sink volume, cell size is the pixel, and 22.13 is the slope length of the standard cell.

2.2.1.4 Vegetation cover management factor. This study uses the method proposed by Van der Knijff et al. (1999) to determine the C factor using NDVI, the equation is expressed as follows:

$$C = \begin{cases} 1 & (f_c = 0) \\ 0.6508 - 0.3436 \lg f_c & (0 < f_c < 78.3\%) \\ 0 & (f_c \geq 78.3\%) \end{cases} \quad (10)$$

$$f_c = \exp\left(-2 \frac{NDVI}{1 - NDVI}\right) \quad (11)$$

where f_c is the vegetation coverage.

2.2.1.5 Water and soil conservation measures factor. The soil and water conservation measure factor is defined as the ratio of the amount of soil loss under a specific water and soil conservation measure to the amount of soil loss when the corresponding measure is not implemented. The value ranges from 0 to 1, with 0 representing the absence of soil erosion and 1 representing the absence of any water conservation practices. The topographic characteristics, farming characteristics, and land use types of the study area were analyzed and previous research results were referenced (Xu and Shao 2006; Chen et al. 2014) to determine the P value of the soil and water conservation measures in the study area.

2.2.2. Theil-Sen median trend analysis and Mann-Kendall significance test

Theil-Sen median trend analysis: It is a robust non-parametric statistical trend method, proposed by Theil in 1950 (Thiel, 1950), and Sen popularized it in 1968 (Sen 1968). The basic estimation idea of this method is that in a univariate linear regression model, first choose two pairs of observations to solve the slope, and then take the median of the slope as the estimated value of the slope parameter. Under the assumption of general random error and random effect distribution, the Theil-Sen estimation is used to obtain the estimation of fixed effect parameters first, and then estimate the variance of random effect and random error, avoiding the use of loop iteration algorithm, simpler calculation, linear

mixing. The applicability of the model is wider, and Theil-Sen estimation is robust (Yang, 2019), and can be used to reflect the changing trend of research elements (Li et al. 2018; Hand et al. 2013) , the equation is expressed as follows:

$$\beta_A = \text{Median}\left(\frac{A_j - A_i}{j - i}\right) \quad 2000 \leq i \leq j \leq 2015 \quad (12)$$

Where β_A is the median of the slope of $n(n-1)/2$ data combinations, A_i and A_j are the average values of pixel A in the i -th and j -th years ($2000 \leq i \leq j \leq 2015$), when $S_A > 0$, indicating that A shows an increasing trend during the study period; on the contrary, it is a degrading trend.

Mann-Kendall significance test: is a non-parametric test method (Hamed and Rao 1998), not easily affected by other factors, suitable for judging whether time series data has an upward or downward trend (Song et al. 2015). the equation is expressed as follows:

Set $\{A_i\}$, $i = 2000, 2001, \dots, 2015$, define the Z statistic as:

$$Z = \begin{cases} \frac{S - 1}{\sqrt{\text{var}(S)}}, & S > 0 \\ 0, & S = 0 \\ \frac{S + 1}{\sqrt{\text{var}(S)}}, & S < 0 \end{cases} \quad (13)$$

$$S = \sum_{j=1}^{n-1} \sum_{i=j+1}^n \text{sgn}(A_j - A_i) \quad (14)$$

$$\text{sgn}(A_j - A_i) = \begin{cases} 1, & A_j - A_i > 0 \\ 0, & A_j - A_i = 0 \\ -1, & A_j - A_i < 0 \end{cases} \quad (15)$$

$$\text{var}(S) = \frac{n(n-1)(2n+5)}{18} \quad (16)$$

A_i and A_j are the average values of pixel A in the i -th and j -th years, n represents the length of the year, and sgn is a sign function. This article judges the significance of the change trend of A at the significance level $\alpha = 0.05$. When the test result $|Z| > 1.96$, it is classified as a significant change, and when $|Z| < 1.96$, it is classified as a slight change (Tian et al. 2015).

Theil-Sen median trend analysis and Mann-Kendall significance test were performed according to the classification in Table 2, reclassified in ArcGis, and then the Con function operation was performed to obtain the degree of evolution trend change.

2.2.3. The relative contribution of precipitation and vegetation to erosion

To further elaborate the relative contribution of precipitation and vegetation to erosion, expressed as the partial derivative of multiple regression, we first use linear regression to

Table 2. Reclassification of Theil-Sen and Mann-Kendall.

Theil-Sen	Mann-Kendall	Degree of change
$S \leq -0.0005$	$Z \leq -1.96$	Significant decreasing
$S \leq -0.0005$	$-1.96 < Z < 1.96$	Slight decreasing
$-0.0005 < S < 0.0005$	$-1.96 < Z < 1.96$	Constant
$S \geq 0.0005$	$-1.96 < Z < 1.96$	Slight increasing
$S \geq 0.0005$	$Z \geq 1.96$	Significant increasing

analyze the actual soil erosion trend (Liu et al. 2019; Chen et al. 2021). Taking the corresponding soil erosion trend as the dependent variable and precipitation and vegetation as the independent variables, the equation is constructed as follows:

$$\frac{d_{Erosion}}{dt} = \frac{d_{Precipitation}}{dt} \times \frac{\partial_{Erosion}}{\partial_{Precipitation}} + \frac{d_{NDVI}}{dt} \times \frac{\partial_{Erosion}}{\partial_{NDVI}} = Precipitation_{con} + NDVI_{con} \quad (17)$$

where $\frac{d_{Erosion}}{dt}$ is the sen median trend of soil erosion change, $\frac{\partial_{Erosion}}{\partial_{Precipitation}}$, $\frac{\partial_{Erosion}}{\partial_{NDVI}}$ represent the large partial derivative between soil erosion and Precipitation and NDVI, respectively. It can be seen from the sheet-related formula that each partial derivative eliminates the influence of other factors. $Precipitation_{con}$ and $NDVI_{con}$ respectively represent the contribution of precipitation and vegetation to erosion.

In order to further distinguish the influence of precipitation and vegetation on soil erosion trends, the relative contribution area of water and vegetation to erosion is generated when calculating according to the formula in Table 3 (Wu et al. 2020).

3. Results and analysis

3.1. Soil erosion changes

The years 2000, 2005, 2010 and 2015 were selected for soil erosion degree and total erosion statistics. The results are shown in Table 4. In terms of erosion area, potential soil erosion showed a decreasing trend, with 10917.25×10^6 ha, 10802.81×10^6 ha, 10819.19×10^6 ha and 10870.69×10^6 ha, respectively. Accounting for 92.86%, 91.88%, 92.02%, 92.46% of the total area of the study area. Light and medium soil erosion showed an increasing trend, with an area of 832.44×10^6 ha, 946.25×10^6 ha, 929.81×10^6 ha, and 877.31×10^6 ha, accounting for 7.08%, 8.05%, 7.91%, and 7.46% of the total area of the study area, respectively. The total area of other erosion is 7.31×10^6 ha, 7.94×10^6 ha, 8.00×10^6 ha, 8.94×10^6 ha, accounting for 0.06%, 0.07%, 0.07% and 0.08% of the total area of the study area. During the study period, the area with erosion levels above light and light soil erosion increased by 44.88×10^6 ha, an increase of 5.39%. It can be seen that the degree of erosion is gradually increasing.

From the distribution of total erosion from 2000 to 2015, the total soil erosion during the study period was 16060.15×10^6 t yr⁻¹, 17397.18×10^6 t yr⁻¹, 17165.62×10^6 t yr⁻¹, 16613.32×10^6 t yr⁻¹, respectively. The total amount showed an increasing trend, an increase of 553.17×10^6 t yr⁻¹, an increase of 3.44%. From the distribution of erosion

Table 3. Eight scenarios for assessing the increase or decrease of soil erosion by precipitation and NDVI.

Type	k	Scenario	Precipitation_ NDVI_		Contribution of Precipitation	Contribution of NDVI
			con	con		
Erosion increasing	$k > 0$	Scenario 1	>0	>0	$\frac{Precipitation_{con}}{ Precipitation_{con} + NDVI_{con} } \times 100$	$\frac{ NDVI_{con} }{ Precipitation_{con} + NDVI_{con} } \times 100$
		Scenario 2	>0	<0	100	0
		Scenario 3	<0	>0	0	100
		Scenario 4	<0	<0	Impossible	Impossible
Erosion decreasing	$k < 0$	Scenario 5	<0	<0	$\frac{Precipitation_{con}}{ Precipitation_{con} + NDVI_{con} } \times 100$	$\frac{ NDVI_{con} }{ Precipitation_{con} + NDVI_{con} } \times 100$
		Scenario 6	<0	>0	100	0
		Scenario 7	>0	<0	0	100
		Scenario 8	>0	>0	Impossible	Impossible

Table 4. Statistics of soil erosion changes over time.

Time (years)	Degree of erosion	Area ($\times 10^6$ ha)	Proportion of area (%)	Average erosion modulus ($t\ ha^{-1}\ yr^{-1}$)	Erosion ($10^6\ t\ yr^{-1}$)	Proportion of erosion (%)
2000	Potential soil erosion	10917.25	92.86	0.58	6332.01	39.43
	Light soil erosion	786.69	6.69	9.82	7725.27	48.10
	Medium soil erosion	45.75	0.39	32.64	1493.28	9.30
	Strength soil erosion	5.75	0.05	60.96	350.52	2.18
	Extremely strength soil erosion	1.56	0.01	101.81	159.08	0.99
	Fierce soil erosion	0.00	0.00	0.00	0.00	0.00
2005	Potential soil erosion	10802.81	91.88	0.58	6265.63	36.02
	Light soil erosion	892.00	7.59	9.93	8857.56	50.91
	Medium soil erosion	54.25	0.46	32.35	1754.99	10.09
	Strength soil erosion	6.75	0.06	59.71	403.04	2.32
	Extremely strength soil erosion	1.19	0.01	97.65	115.96	0.67
	Fierce soil erosion	0.00	0.00	0.00	0.00	0.00
2010	Potential soil erosion	10819.19	92.02	0.58	6275.13	36.56
	Light soil erosion	876.94	7.46	9.84	8629.07	50.27
	Medium soil erosion	52.88	0.45	32.57	1722.14	10.03
	Strength soil erosion	6.38	0.05	59.33	378.23	2.20
	Extremely strength soil erosion	1.63	0.01	99.11	161.05	0.94
	Fierce soil erosion	0.00	0.00	0.00	0.00	0.00
2015	Potential soil erosion	10870.69	92.46	0.55	5978.88	35.99
	Light soil erosion	820.31	6.98	9.93	8145.70	49.03
	Medium soil erosion	57.00	0.48	33.24	1894.68	11.40
	Strength soil erosion	7.81	0.07	60.24	470.63	2.83
	Extremely strength soil erosion	1.13	0.01	100.61	113.19	0.68
	Fierce soil erosion	0.06	0.00	163.96	10.25	0.06

amount of different Erosion grades, the distribution of potential soil erosion was the largest, but gradually decreased during the study period. There were $6332.01 \times 10^6\ t\ yr^{-1}$, $6265.63 \times 10^6\ t\ yr^{-1}$, $6275.13 \times 10^6\ t\ yr^{-1}$ and $5978.88 \times 10^6\ t\ yr^{-1}$, respectively. Light and medium soil erosion have $9218.55 \times 10^6\ t\ yr^{-1}$, $10612.55 \times 10^6\ t\ yr^{-1}$, $10351.20 \times 10^6\ t\ yr^{-1}$, and $10040.38 \times 10^6\ t\ yr^{-1}$, respectively, an increase of $821.83 \times 10^6\ t\ yr^{-1}$, an increase of 8.91%. The total erosion of strength and strength above grades is $509.60 \times 10^6\ t\ yr^{-1}$, $519.00 \times 10^6\ t\ yr^{-1}$, $539.28 \times 10^6\ t\ yr^{-1}$ and $594.06 \times 10^6\ t\ yr^{-1}$, an increase of $1.17 \times 10^6\ t\ yr^{-1}$, an increase of 0.23%.

From the above analysis, during 2000 analysis and 2015, except for the reduction of potential soil erosion area and erosion amount, the erosion area and erosion amount of other grades showed an increasing trend, of which light and light grades had the largest amount of erosion.

3.2. Spatial distribution of soil erosion

3.2.1. Distribution on the continents

It can be seen from Figure 1 that during 2000-2015, soil erosion in Africa and North America showed an increasing trend, and the Pearson correlation coefficient R^2 was 0.036 and 0.1361, respectively. From 2000 to 2010, the global urban land expansion rate was much faster than expected. North America's urban expansion area was large. In addition, the expansion of new urbanization in Africa accounted for about 12% of the total urban area of the African continent (Robinson et al. 2017). Therefore, the increase in erosion

area during this period may be related to potential driving forces such as population growth. The erosion in Asia, Europe, South America and Oceania all showed a downward trend, and the Pearson correlation coefficient R^2 was 0.0204, 0.3941, 0.3773 and 0.1222, respectively. It can be seen from Figure 1 that the decline in soil erosion changes in Europe is the most obvious. Judging from the distribution of mean erosion modulus for many years, Asia has the largest erosion modulus ($>2.00 \text{ t ha}^{-1} \text{ yr}^{-1}$), followed by North America. The mean erosion modulus distribution ranges from 1.45 to $1.80 \text{ t ha}^{-1} \text{ yr}^{-1}$.

From the changes in the soil erosion modulus time, it can be seen that in 2011, Africa and Europe had the lowest erosion modulus during the study period, and Asia had the lowest erosion modulus in 2001. There was a sharp increase in the following two years, and then fluctuations decreased. North America had the lowest erosion modulus in 2004, and since then, the overall volatility has increased. There were two low values in Oceania in 2005 and 2013, and they showed a steady decline during the period 2006-2012. In South America, the soil erosion modulus dropped sharply in 2002, after which the erosion

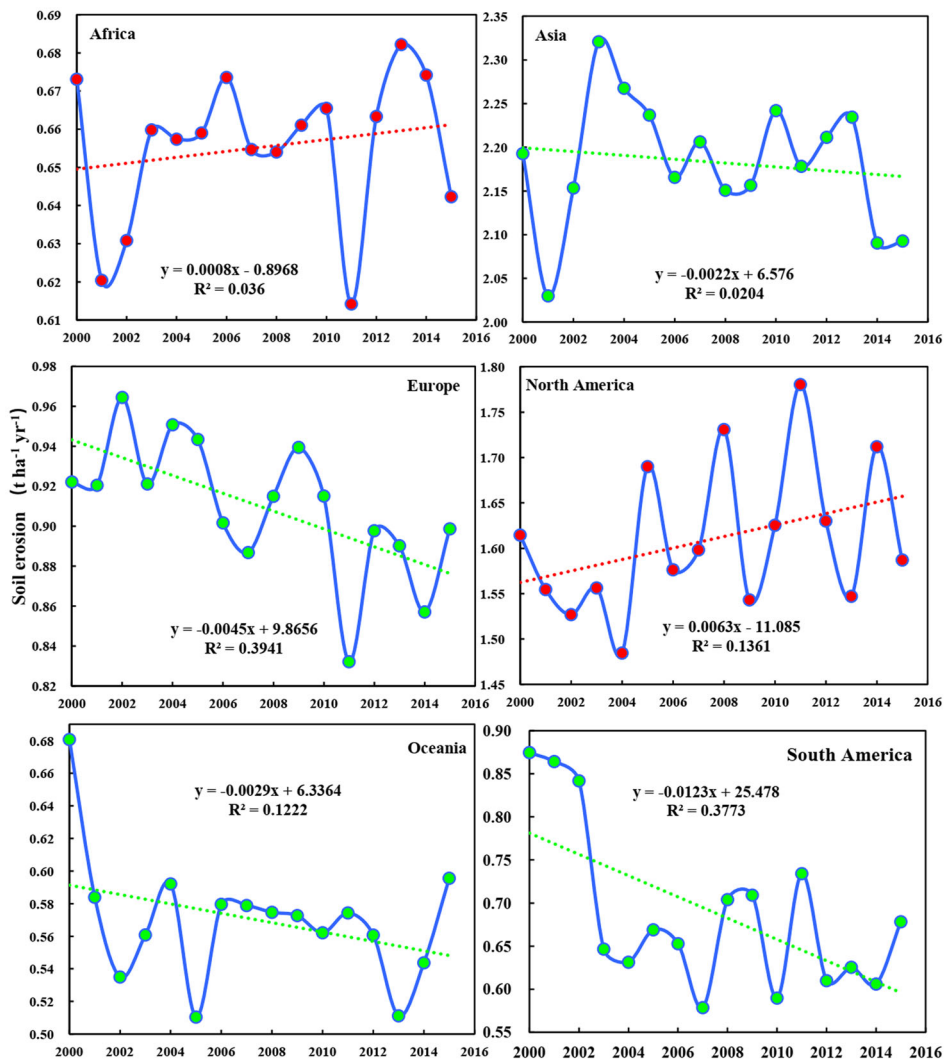


Figure 1. The temporal and spatial distribution of soil erosion from 1996 to 2015.

modulus changed between 0.55 and 0.75 t ha⁻¹yr⁻¹, and reached the lowest value of erosion modulus in 2007 and the highest value in 2011.

3.2.2. Distribution on the climatic zone

Soil erosion in different climatic zones has strong spatial distribution differences (Figure 2). In general, the tropical, arid zone, warm temperate zone and cold temperate zone account for 19.86%, 20.50%, 15.40% and 44.24% of the area respectively. The soil erosion modulus is lower than 0.25 t ha⁻¹yr⁻¹, mainly distributed in tropical monsoon climate (Am), accounting for 3.51% of the area. The soil erosion modulus is 0.25–0.50 t ha⁻¹yr⁻¹, mainly concentrated in tropical rain forest climate (Af), tropical open forest grassland climate (Aw) and summer hot normal humidity and warm climate (Cfa), and the area accounts for 16.35%. The soil erosion modulus is 0.50–0.80 t ha⁻¹yr⁻¹, which is mainly distributed in hot summer/subtropical monsoon humid climate (Cwa), hot summer warm temperate climate (Cfa) and hot summer climate (Dfa), The area accounts for 11.11%. The soil erosion modulus is 0.80–0.15 t ha⁻¹yr⁻¹, mainly concentrated in tropical desert climate (Bwh), savanna climate (Bsh), hot summer and normal humidity and warm climate (Cfa), hot summer and dry winter Cold temperature climate (Dwa) and summer cool normal humidity and cold temperature climate (Dfc) account for 29.06% of the area. On the whole, the soil erosion modulus is greater than 0.15 t ha⁻¹yr⁻¹, and the

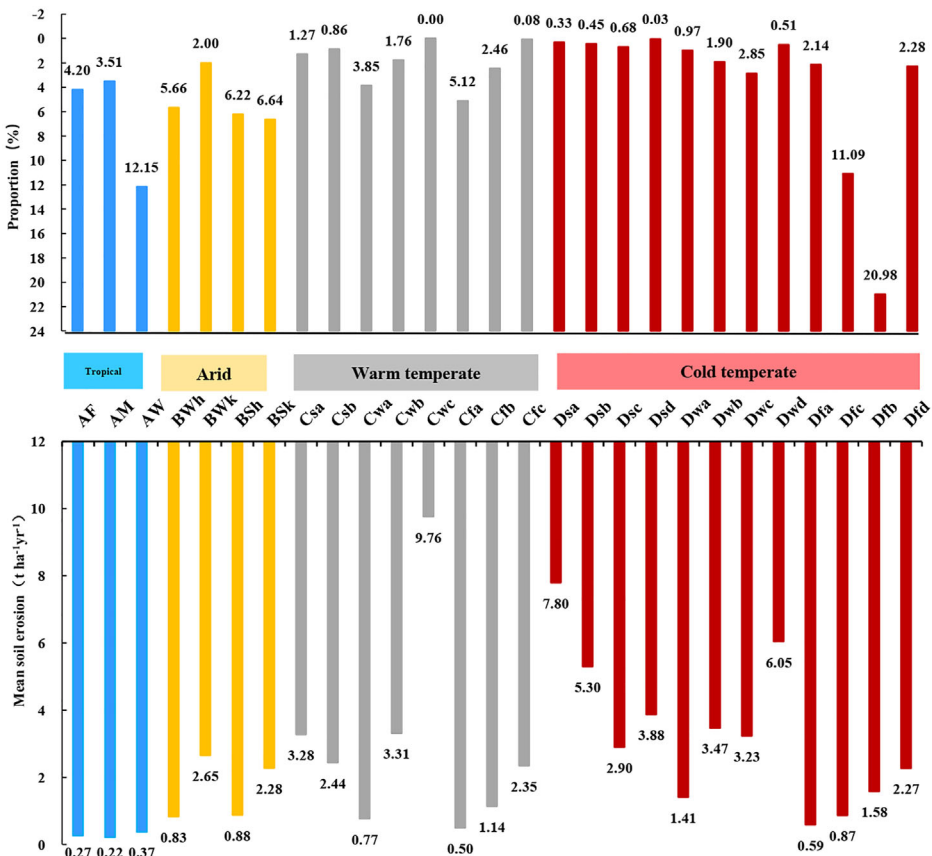


Figure 2. Spatial distribution of soil erosion in different climatic zones.

degree of erosion is intense, mainly distributed in the warm temperate zone and the cold temperate zone, accounting for 39.97% of the area.

3.3. Soil erosion trend analysis

The soil erosion Theil-Sen median trend analysis and Mann-Kendall significance test comprehensively analyzed the soil erosion evolution trend based on the pixel scale (Figure 3). Figure 3(b) shows that the more widely distributed types of soil erosion evolution trends are ‘Slight decreasing’(39.00%) and ‘Slight increasing’ (38.34%), followed by ‘Significant decreasing’ (11.51%) and ‘Significant increasing’ (6.93%), The least is the ‘Constant’(4.22%). In addition, the analysis of the spatial change of the evolution trend of soil erosion shows (Figure 3a) that the areas where soil erosion has been significantly decreasing are mainly concentrated in Asia and Europe. In these areas, the significant decreasing in soil erosion in China is more obvious. This may be related to China’s return of farmland to forests. The implementation of grass and other ecological projects (Tong et al. 2018; Chen et al. 2019; Liu et al. 2021). The areas with significant increasing in soil erosion are mainly distributed in a country on the border of the United States, eastern Russia, Congo, Kazakhstan and Russia, and in northern Africa next to the Sahara Desert. The ‘Constant’ is mainly distributed in the Amazon plain.

3.4. The impact of precipitation and vegetation on erosion

3.4.1. Evolution characteristics of precipitation and vegetation

Based on the pixel-scale rainfall evolution trend analysis (Figure 4a), combined with Theil-Sen median trend analysis and Mann-Kendall test (Table 2). The results show that the precipitation evolution types of the two widely distributed are ‘Slight increasing’ (44.28%) and ‘Significant increasing’ (24.43%), followed by ‘Slight decreasing’(18.79%) and ‘Constant’ (8.17%), the least is ‘Significant decreasing’(4.33%) (Figure 4b). In addition, the analysis of spatial changes in precipitation trends shows that there has been a significant increase in widespread rainfall, mainly in Russia, Kazakhstan, northern China, Pakistan, India, Finland, Alaska, Mexico and Peru. However, the areas with a significant decreasing in precipitation are mainly distributed in the western and southern coastal areas of North America, southern Africa, the Himalayas and New Zealand.

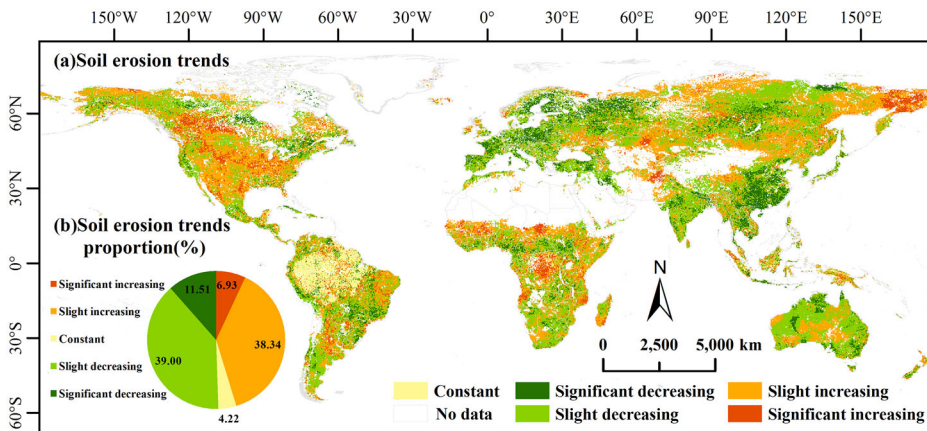


Figure 3. Changes in the evolution trend of soil erosion.

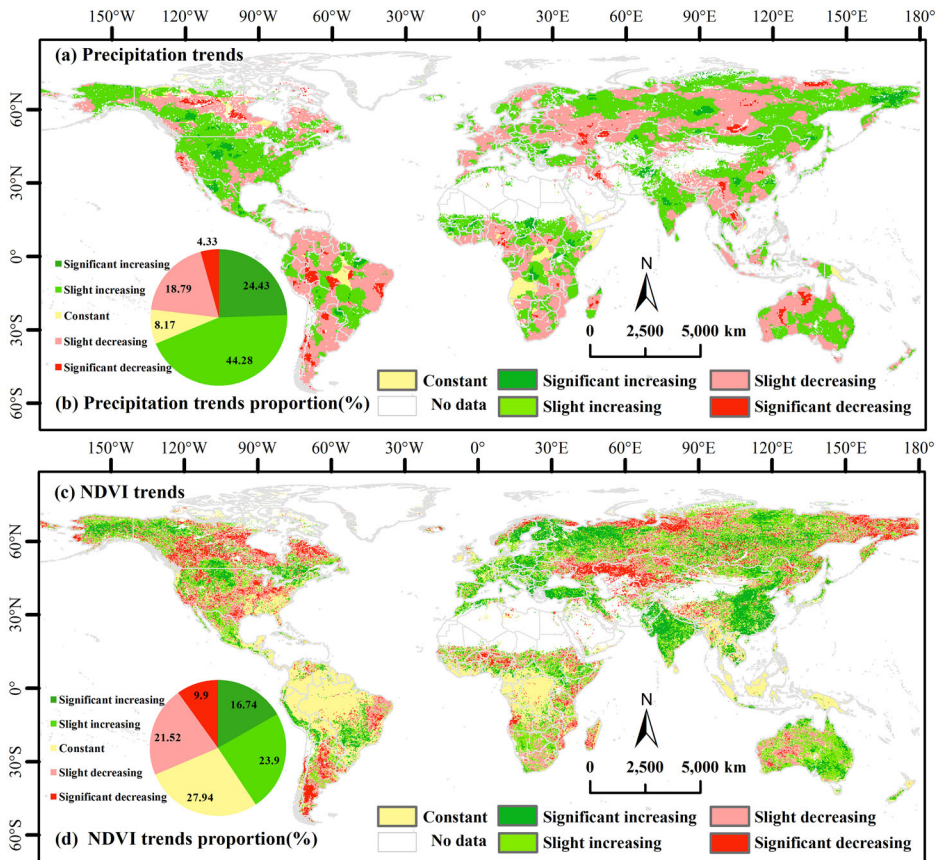


Figure 4. Variation trend of precipitation and vegetation.

The results show (Figure 4c and d) that the NDVI evolution types of the two widely distributed are ‘Constant’ (27.94%), ‘Slight increasing’ (23.90%), followed by ‘Slight decreasing’ (21.52%) and ‘Significant increasing’ (16.74%), the least is ‘Significant decreasing’ (9.90%). Therefore, analyses of the changes in vegetation show a widespread greening trend (the area accounts for 40.64%), these are mainly observed in the Europe, India and south China. In the Amazon Basin, Congo Basin, and Southeast Asia, the vegetation changes are not obvious and relatively ‘Constant’. The vegetation also show decreasing NDVI trend (the area accounts for 31.42%), and these are observed near Canada, South America and Central Asia.

3.4.2. The relative contribution of precipitation and vegetation to erosion

Contribution of precipitation to soil erosion, from the perspective of the negative contribution of precipitation to the occurrence of soil erosion (Figure 5a and b), the area accounts for the largest proportion of $0 - -0.3 \text{ t ha}^{-1}\text{yr}^{-1}$ (14.20%), followed by $< -1 \text{ t ha}^{-1}\text{yr}^{-1}$ (5.68%), $-0.5 - -1 \text{ t ha}^{-1}\text{yr}^{-1}$ (5.30%) and $-0.3 - -0.5 \text{ t ha}^{-1}\text{yr}^{-1}$ (3.94%). It is mainly distributed in small countries such as New Zealand, Ecuador, Mozambique, Colombia, Venezuela, Guyana, Suriname, Liberia, Sierra Leone, Myanmar, Bangladesh, Nepal and Iceland, as well as the areas bordering the United States, Canada, Australia, China and India. From the perspective of the positive contribution of precipitation to soil erosion (Figure 5a and b), the area accounts for the largest proportion of $0.5 -$

1 t ha⁻¹yr⁻¹ (23.87%), followed by >1 t ha⁻¹yr⁻¹ (20.28%), 0-0.3 t ha⁻¹yr⁻¹ (15.66%) and >0.3-0.5 t ha⁻¹yr⁻¹ (11.07%). In central Russia, Finland, northern Kazakhstan, India, western Canada, Alaska, Mexico and Argentina.

Contribution of vegetation to soil erosion: 53.81% of the vegetation contributes negatively to the occurrence of soil erosion, on the contrary, 46.19% of the vegetation contributes to the occurrence of soil erosion. From the perspective of the negative contribution of NDVI to soil erosion (Figure 5c and d), the area accounted for the largest proportion of -0.0015— -0 t ha⁻¹yr⁻¹ (33.65%), followed by -0.0025— -0.0015 t ha⁻¹yr⁻¹ (9.79%), -0.0025— -0.0035 t ha⁻¹yr⁻¹ (5.30%) and <-0.0035 t ha⁻¹yr⁻¹ (5.07%). NDVI has the most significant negative contribution to soil erosion in northern and central North America, northwestern Europe, eastern and southwestern China, India and southeastern Australia. Affected by the ocean, Europe and Australia have abundant rainfall and good vegetation growth. In addition, vegetation in China and India is turning green (Chen et al. 2019), and China's ecological engineering has played a large role in the process of vegetation turning green (Tong et al. 2018). It shows that where vegetation grows better, soil and water conservation is better, and erosion is not easy to occur.

From the perspective of the positive contribution of vegetation (NDVI) to the occurrence of soil erosion (Figure 5c and d), the area with the largest proportion is 0—0.0015 t ha⁻¹yr⁻¹ (31.36%), followed by 0.0015—0.0025 t ha⁻¹yr⁻¹ (8.47%), 0.0025—0.0035 t ha⁻¹yr⁻¹ (3.60%) and > 0.0035 t ha⁻¹yr⁻¹ (2.77%). On the borders of Argentina,

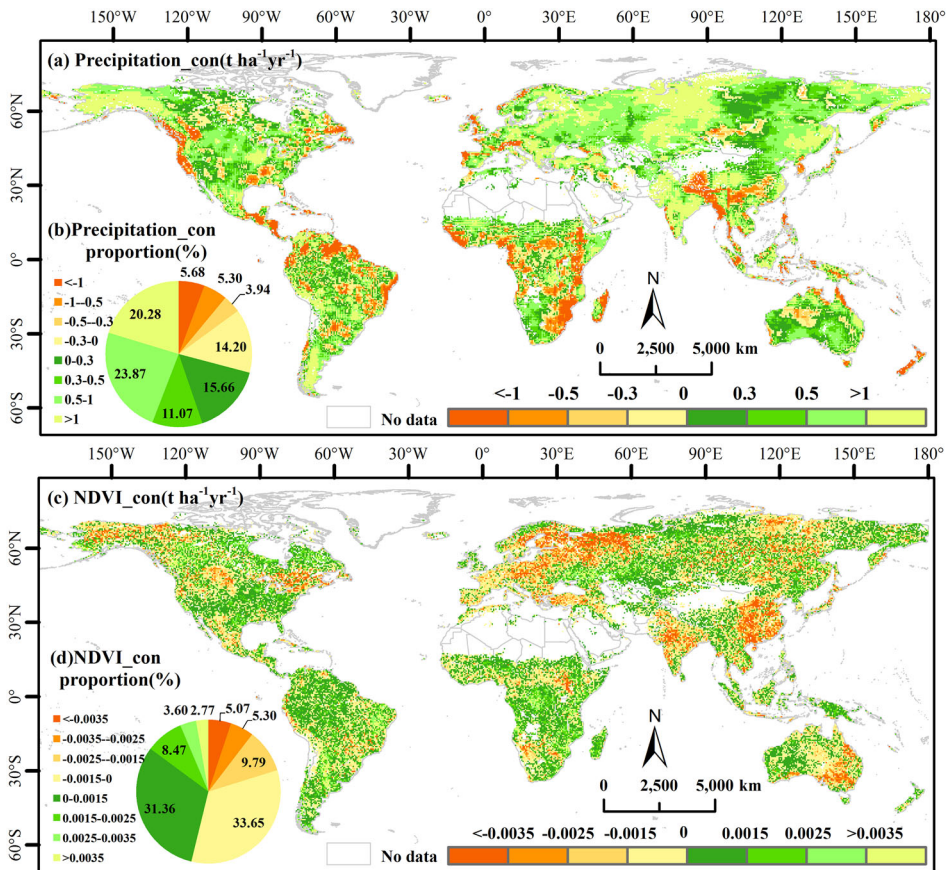


Figure 5. The spatial distribution of the contribution of precipitation and vegetation to soil erosion.

eastern Brazil, Congo, Tanzania, Kazakhstan, and Russia, NDVI has the most obvious positive contribution to soil erosion. High temperatures in these areas may cause soil moisture to evaporate and decrease soil moisture (Yang et al. 2019; Deng et al. 2020). In this case, the plant suffers from physiological drought, which limits the photosynthesis and growth rate of the plant (Piao et al. 2007). Poor water and soil conservation is prone to soil erosion.

Figure 6 shows the change trend of soil erosion. Precipitation dominates the occurrence of erosion in 88.49% of the area, and vegetation accounts for only 11.51% (Figure 6a and b). In areas where soil erosion shows a decreasing trend, precipitation is still the main controlling factor, dominating the erosion in 61.43% of the area, and vegetation controlling 38.57% (Figure 6c and d).

4. Discussion

4.1. Comparison of rainfall erosivity with other studies

The maximum rainfall erosion from 2000 to 2015 varied from 17126.50 to 26169.20 MJ mm ha⁻¹ h⁻¹ yr⁻¹. The maximum rainfall erosivity in 2015 was the lowest, and the maximum rainfall erosivity in 2008 was the highest

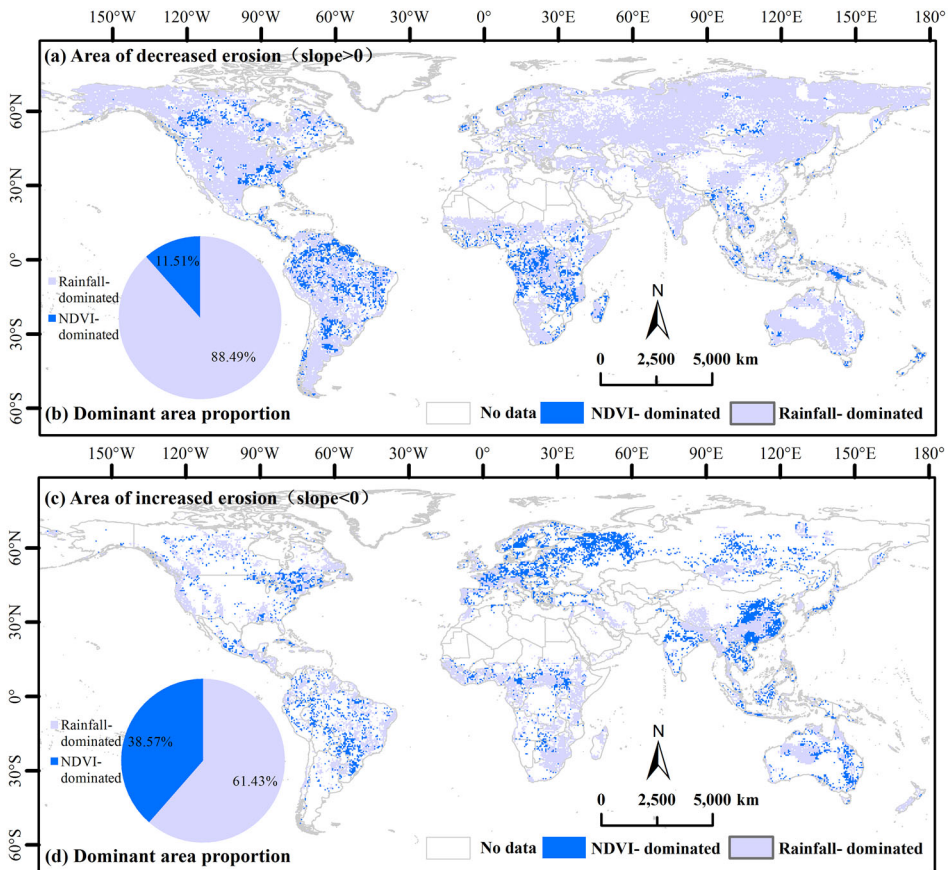


Figure 6. Contribution of precipitation and vegetation to soil erosion.

Table 5. Rainfall erosivity distribution on different continents (Unit: MJ mm ha⁻¹ h⁻¹ yr⁻¹).

Continents	Africa	Asia	Europe	North America	Oceania	South America
Max	11428.45	17682.29	9835.65	13439.02	14183.74	18208.54
Mean	4606.52	3266.01	2990.96	3005.71	3054.12	5975.16

In North America, the average rainfall erosivity is 3005.71 MJ mm ha⁻¹ h⁻¹ yr⁻¹ (Table 5), and the average rainfall erosivity in Canada is 2582.29 MJ mm ha⁻¹ h⁻¹ yr⁻¹ (Supporting Material Table 1). The average rainfall erosivity in the United States is 3056.446 MJ mm ha⁻¹ h⁻¹ yr⁻¹, the average rainfall erosivity in Mexico is 4021.378 MJ mm ha⁻¹ h⁻¹ yr⁻¹, and the rainfall erosivity in Central America is >7000 MJ mm ha⁻¹ h⁻¹ yr⁻¹.

In South America, the maximum average rainfall erosivity is 5975.16 MJ mm ha⁻¹ h⁻¹ yr⁻¹ (Table 5). Unlike previous studies that Chile has the lowest rainfall erosivity (Panagos et al. 2017), the results of this study show that Argentina has the lowest average rainfall factor (2851.38 MJ mm ha⁻¹ h⁻¹ yr⁻¹) (Supporting Material Table 1), Followed by Chile (3618.14 MJ mm ha⁻¹ h⁻¹ yr⁻¹). High rainfall erosivity in South America is mainly concentrated in Brazil (6747.33 MJ mm ha⁻¹ h⁻¹ yr⁻¹), Colombia, Ecuador and Venezuela (>7483.49 MJ mm ha⁻¹ h⁻¹ yr⁻¹).

In Europe, the maximum rainfall erosivity is 9835.65 MJ mm ha⁻¹ h⁻¹ yr⁻¹, and the average value is 2990.96 MJ mm ha⁻¹ h⁻¹ yr⁻¹. In Africa, the average rainfall erosivity is 4,066.52 MJ mm ha⁻¹ h⁻¹ yr⁻¹. The high rainfall erosivity (>8000 MJ mm ha⁻¹ h⁻¹ yr⁻¹) (Supporting Material Table 1) is mainly distributed in Liberia, Sierra Leone and Guinea in West Africa. Areas with low rainfall erosivity (<3000 MJ mm ha⁻¹ h⁻¹ yr⁻¹) are mainly concentrated in South Africa and Somalia.

In Asia, the average rainfall erosivity is 3266.01 MJ mm ha⁻¹ h⁻¹ yr⁻¹ (Table 5). Russia, Kazakhstan, Inner Mongolia, and the Middle East have low rainfall erosivity, which is similar to the spatial distribution pattern of global rainfall erosivity assessment based on high temporal resolution rainfall records by Panagos et al. (2017). The average rainfall erosivity of China is 3576.09 MJ mm ha⁻¹ h⁻¹ yr⁻¹ (Supporting Material Table 1), showing a trend of increasing from northwest to southeast, showing strong rainfall erosivity in the southeast coast (>8000 MJ mm ha⁻¹ h⁻¹ yr⁻¹). Rainfall erosivity in Southeast Asia > 10000 MJ mm ha⁻¹ h⁻¹ yr⁻¹. The average rainfall erosivity in Japan is 5911.45 MJ mm ha⁻¹ h⁻¹ yr⁻¹, which is slightly higher than the 5130 MJ mm ha⁻¹ h⁻¹ yr⁻¹ studied by other scholars (Shiono et al. 2013).

The average rainfall erosivity in Oceania is 3054.12 MJ mm ha⁻¹ h⁻¹ yr⁻¹ (Table 5). The average rainfall erosivity in Australia is 2884.69 MJ mm ha⁻¹ h⁻¹ yr⁻¹ (Supporting Material Table 1), which is higher than the 1767 MJ mm ha⁻¹ h⁻¹ yr⁻¹ estimated by Teng et al. (2016) based on 11 years (2002-2012). In addition, they also found that the maximum erodibility in the northern and eastern coastal areas is greater than 8000 MJ mm ha⁻¹ h⁻¹ yr⁻¹, and decreases toward the central and southern areas (Teng et al., 2016). In New Zealand, rainfall erosivity is greater than 5000 MJ mm ha⁻¹ h⁻¹ yr⁻¹, occurring on the southeastern coast of New Zealand and gradually increasing to the northwest. It is similar to the pattern observed by Klik et al. (2015) based on 35 weather stations.

4.2. Effects of vegetation on soil erosion

Vegetation cover is an important soil and water conservation measure, which can significantly increase runoff resistance, slow down and delay the flow rate of runoff, weaken the shear force and power of runoff on the slope, and reduce the soil erosion degree. In our

study, we found that NDVI value of the area on the upward trend were Europe, India and China, while the area on the downward trend Canada, South America and Central Asia (Figure 4). In areas where vegetation is increasing, soil erosion is correspondingly decreasing (Figure 3). This is consistent with related research, Chen et al. found that China and India lead the global greening mainly because of China's tree planting plan and the intensive agriculture of China and India (Chen et al. 2019). Liu and Lei (2015) analyzed the cumulative afforestation area and NDVI changes in China's returning farmland to forest project over the years, and found that since the implementation of the project of returning farmland to forests and grassland in 1999, China's afforestation area has continued to rise, and NDVI has also shown an increasing. It shows that the implementation of ecological restoration projects in recent years has greatly promoted the increase of vegetation cover in China and achieved good results (Yang et al. 2019). From the perspective of the relative influence of vegetation on erosion, the increase of vegetation is not conducive to soil and water conservation in 46.19% of areas (Figure 5c and d). High temperatures in these areas may cause soil moisture to evaporate and decrease soil moisture (Yang et al. 2019; Deng et al. 2020). In this case, plants will experience physiological drought, which limits the photosynthesis and growth rate of plants (Piao et al. 2007), it is prone to soil erosion.

4.3. Effect of precipitation on soil erosion

In the process of rainfall, the slope soil is mechanically hit and dissipated by raindrops. The deposition of fine soil particles on the soil surface leads to the formation of surface crust on the soil surface, which promotes the occurrence of surface runoff and results in slope erosion (Assouline 2004). In our study, rainfall promoted erosion in central Russia, Finland, northern Kazakhstan, India, western Canada, Alaska, Mexico and Argentina (Figure 5a and b). Excessive precipitation in these areas leads to increased cloud cover, reduced incident radiation and increased soil moisture, which is not conducive to the growth of vegetation and leads to erosion. In the area of erosion increase, the area dominated by rainfall accounted for 88.49% (Figure 6). Most of these places have sparse vegetation cover, and water is the most important factor limiting the growth of vegetation in the area, so erosion is more likely to occur (Yang et al. 2019). The negative contribution of precipitation to erosion accounts for 29.12%, in these areas, vegetation is constant, and precipitation can maintain the stability of vegetation change, and play the role of soil and water conservation. In this case, the erosion caused by precipitation is small or insignificant (Wang 2018). Therefore, precipitation inhibits the occurrence of erosion and makes a negative contribution.

4.4. Uncertainty

By relying on a ratio of band intensities, NDVI removes a large proportion of noise caused by cloud shadows, topographic and solar angle variations, and atmospheric attenuations existing in visible red and infrared bands, which makes NDVI less susceptible to illumination conditions (Kumari et al. 2020). While varying illumination conditions caused by topography have been observed to have negligible impacts on NDVI applications due to its band ratio format (Matsushita et al. 2007), they still can produce some bias especially on rugged, steep terrain with low solar angles (Kumari et al. 2020), and the recent paper shows that changes in vegetation phenology can be better captured using the EVI than the NDVI (Kumari et al. 2021). The conversion from natural to agricultural

land use removes the protective cover of natural vegetation and this typically increases soil erosion by one to two orders of magnitude (Montgomery 2007), thereby accelerating physical erosion well over equilibrium levels. However, the spatial resolution used in our study was $0.25^{\circ} \times 0.25^{\circ}$, which resulting in a low topographic factor LS, leading to differences in the spatial distribution of soil erosion in individual places compared with previous studies. In this case, our results are relatively lower than the high-resolution (250×250 m) erosion results of other scholars (Borrelli et al. 2017).

5. Conclusion

In order to estimate global soil erosion and understand the impact of precipitation and vegetation on erosion, we used the RUSLE model to estimate the distribution pattern of erosion, showing that erosion is mainly distributed in Asia and North America, and is most widely distributed in the temperate zone. Trend analysis shows that 70.80% of the area shows an increasing trend of erosion, vegetation and precipitation increased significantly in 16.74% and 24.43% areas, respectively. The relative contribution analysis showed that the negative contribution of precipitation and vegetation to erosion accounted for 29.12% and 53.81%, respectively. Therefore, increased precipitation weakens the positive effect of vegetation greening on erosion.

Author Contributions

Conceptualization, Xiaoyong Bai; Data curation, Xuling Luo; Formal analysis, Xuling Luo, Chaoyong Shen; Investigation, Xuling Luo and Yu Zhang; Methodology, Xuling Luo and Luhua Wu; Validation, Xuling Luo and Fei Chen; Visualization, Xuling Luo, Chen Ran and Min Liu; Writing – original draft, Xuling Luo; Revised, Xuling Luo, Ruidong Yang and Yue Cao. All authors have read and agreed to the published version of the manuscript.

Disclosure statement

No potential conflict of interest was reported by the authors.

Funding

This research work was supported jointly by the Western Light Cross-team Program of Chinese Academy of Sciences (xbzg-zdsys-202101), National Natural Science Foundation of China (42077455), Strategic Priority Research Program of the Chinese Academy of Sciences (XDB40000000 & XDA23060100), Guizhou Provincial Science and Technology Projects (2022-198), High-level innovative talents in Guizhou Province (GCC[2022]015-1), Opening Fund of the State Key Laboratory of Environmental Geochemistry (SKLEG2022206 & SKLEG2022208), The Outstanding Youth Science and Technology program of Guizhou Province of China ([2021]5615).

ORCID

Xiaoyong Bai  <http://orcid.org/0000-0001-9705-5574>

Data availability statement

I promise that Availability of Data and Material is available.

References

- Alewell C, Borrelli P, Meusburger K, Panagos P. 2019. Using the USLE: chances, challenges and limitations of soil erosion modelling. *Int Soil Water Conserv Res.* 7(3):203–225.
- Alewell C, Rengeval B, Ballabi C, Robinson DA, Panagos P, Borrelli P. 2020. Global phosphorus shortage will be aggravated by soil erosion. *Nat Commun.* 11(1):4546.
- Assouline S. 2004. Rainfall-induced soil surface sealing: a critical review of observations, conceptual models, and solutions. *Vadose Zone J.* 3(2):570–591.
- Bai X, Zhang S, Li C, Xiong L, Song F, Du C, Li M, Luo Q, Xue Y, Wang S. 2023. A carbon neutrality capacity index for evaluating carbon sink contributions. *Environ Sci Ecotechnol.* 100237.
- Borrelli P, Robinson DA, Fleischer LR, Lugato E, Ballabio C, Alewell C, Meusburger K, Modugno S, Schütt B, Ferro V, et al. 2017. An assessment of the global impact of 21st century land use change on soil erosion. *Nat Commun.* 8(1):1–13.
- Borrelli P, Robinson DA, Panagos P, Lugato E, Yang JE, Alewell C, Wuepper D, Montanarella L, Ballabio C. 2020. Land use and climate change impacts on global soil erosion by water (2015–2070). *Proc Natl Acad Sci U S A.* 117(36):21994–22001.
- Cao SX, Chen L, Shankman D, Wang CM, Wang XB, Zhang H. 2011. Excessive reliance on afforestation in China's arid and semi-arid regions: lessons in ecological restoration. *Earth Sci Rev.* 104(4):240–245.
- Cao SX, Wang GS, Chen L. 2010. Questionable value of planting thirsty trees in dry regions. *Nature.* 465(7294):31.
- Chappell A, Baldock J, Sanderman J. 2016. The global significance of omitting soil erosion from soil organic carbon cycling schemes. *Nat Clim Change.* 6(2):187–191.
- Chappell A, Rossel R, Loughran R. 2011. Spatial uncertainty of ¹³⁷Cs-derived net (1950s–1990) soil redistribution for Australia. *J Geophys Res.* 116.
- Chappell A, Sanderman J, Thomas M, Read A, , Leslie C. 2012. The dynamics of soil redistribution and the implications for soil organic carbon accounting in agricultural south-eastern Australia. *Glob Change Biol.* 18(6):2081–2088.
- Chen C, Park T, Wang XH, Piao SL, Xu BD, Chaturvedi RK, Fuchs R, Brovkin V, Ciais P, Fensholt R, et al. 2019. China and india lead in greening of the world through land-use management. *Nat Sustain.* 2:122–129.
- Chen H, Bai XY, Li YB, Li Q, Wu LH, Chen F, Li CJ, Deng YH, Xi HP, Ran C, et al. 2021. Soil drying weakens the positive effect of climate factors on global gross primary production. *Ecol Indic.* 129(3): 107953.
- Chen SX, Yang XH, Xiao LL, Cai HY. 2014. Study of soil erosion in the southern hillside Area of China based on RUSLE model. *Resour Sci.* 36(06):1288–1297.
- David P, Michael B. 2013. Soil erosion threatens food production. *Agriculture.* 3(3):443–463.
- Deng YH, Wang SJ, Bai XY, Luo GJ, Wu LL, Chen F, Wang JF, Li CJ, Yang YJ, Hu ZY, et al. 2020. Vegetation greening intensified soil drying in some semi-arid and arid areas of the world. *Agric for Meteorol.* 292:108103.
- Diodato N, Bellocchi G. 2007. Estimating monthly (R) USLE climate input in a Mediterranean region using limited data. *J Hydrol.* 345(3–4):224–236.
- Doetterl S, Berhe AA, Nadeu E, Wang Z, Sommer M, Fiener P. 2016. Erosion, deposition and soil carbon: a review of process-level controls, experimental tools and models to address C cycling in dynamic landscapes. *Earth Sci Rev.* 154:102–122.
- FAO.1971-1981. Soil Map of the World(1:5 M). UNESCO, Paris. 110.
- FAO/IIASA/ISRIC/ISSCAS/JRC. 2012. Harmonized World Soil Database (version 1.2). FAO, Rome, Italy and IIASA, Laxenburg, Austria.
- FeNG XM, Sun G, Fu BJ, Su CH, Liu Y, Lamparski H. 2012. Regional effects of vegetation restoration on water yield across the Loess Plateau, China. *Hydrol Earth Syst Sci.* 16(8):2617–2628.
- Fischer G, Nachtergaele F, Prieler S, van Velthuisen HT, Verelst L, Wiberg D. 2008. Global agro-ecological zones assessment for agriculture (GAEZ 2008). IIASA, Laxenburg, Austria and FAO, Rome, Italy.
- Hamed KH, Rao AR. 1998. A modified Mann-Kendall trend test for autocorrelated data. *J Hydrol.* 204(1–4):182–196.
- Hamilton BM, Selby MJ. 1982. Hillslope materials and processes. *Trans Inst Br Geogr.* 19(4):505.
- Hand JL, Schichtel BA, Malm WC, Frank NH. 2013. Spatial and temporal trends in PM_{2.5} organic and elemental carbon across the United States. *Adv Meteorol.* 2013:1–13.
- Hartley AJ, MacBean N, Georgievski G, Bontemps S. 2017. Uncertainty in plant functional type distributions and its impact on land surface models. *Remote Sens Environ.* 203:71–89.

- Kaufmann RK, Zhou L, Tucker CJ, Slayback D, Shabanov NV, Myneni RB. 2002. Variations in northern vegetation activity inferred from satellite data of vegetation index during 1981 to 1999. *J Geophys Res Atmos.* 107(D11):ACL-1-ACL 7-3.
- Klik A, Haas K, Dvorackova A, Fuller IC. 2015. Spatial and temporal distribution of rainfall erosivity in New Zealand. *Soil Res.* 53(7):815–825.
- Kumari N, Saco PM, Rodriguez JF, Johnstone SA, Srivastava A, Chun KP, Yetemen O. 2020. The grass is not always greener on the other side: seasonal reversal of vegetation greenness in aspect-driven semi-arid ecosystems. *Geophys Res Lett.* 47(15):e2020GL088918.
- Kumari N, Srivastava A, Dumka UC. 2021. A long-term spatiotemporal analysis of vegetation greenness over the Himalayan region using Google earth engine. *Climate.* 9(7):109.
- Lal R. 1990. Soil erosion and land degradation: the global risks. In *Advances in soil science*. New York, NY: Springer; p. 129–172.
- Lal R, Stewart BA. 1990. *Soil Degradation*. New York: Springer-Verlag.
- Lal R. 2003. Soil erosion and the global carbon budget. *Environ Int.* 29(4):437–450.
- Langbein WB, Schumm SA. 1958. Yield of sediment in relation to mean annual precipitation. *Trans AGU.* 39(6):1076–1084.
- Li M, Chu R, Shen S, Islam ARMT. 2018. Dynamic analysis of pan evaporation variations in the Huai River Basin, a climate transition zone in eastern China. *Sci Total Environ.* 625:496–509.
- Liu BY, Nearing MA, Risse LM. 1994. Slope gradient effects on soil loss for steep slopes. *Trans ASAE.* 37(6):1835–1840.
- Liu C, Wang D, Dong FF, Hu BX, Li ZW, Huang B. 2021. Modeling organic matter sources of sediment fluxes in eroding landscapes: review, key challenges, and new perspectives. *Geoderma.* 383:114704.
- Liu M, Bai XY, Tan Q, Luo GJ, Zhao CW, Wu LH, Hu ZY, Ran C, Deng YH. 2021. Monitoring impacts of ecological engineering on ecosystem services with Geospatial Techniques in karst areas of SW China. *Geocarto Int.* 37(17):5091–5115.
- Liu XP, Pei FS, We YY, Li X, Wang SJ, Wu CJ, Cai YL, Wu JG, Chen J, Feng KS, et al. 2019. Global urban expansion offsets climate-driven increases in terrestrial net primary productivity. *Nat Commun.* 10(1):5558.
- Liu Y, Lei H. 2015. Responses of natural vegetation dynamics to climate drivers in China from 1982 to 2011. *Remote Sens.* 7(8):10243–10268.
- Liu YX, Fu BJ, Liu Y, Zhao WW, Wang S. 2019. Vulnerability assessment of the global water erosion tendency: vegetation greening can partly offset increasing rainfall stress. *Land Degrad Dev.* 30(9):1061–1069.
- Lugato E, Smith P, Borrelli P, Panagos P, Ballabio C, Orgiazzi A, Fernández-Ugalde O, Montanarella L, Jones A. 2018. Soil erosion is unlikely to drive a future carbon sink in Europe. *Sci Adv.* 4(11):eaau3523.
- Luo X, Bai X, Tan Q, Ran C, Chen H, Xi H, Chen F, Wu L, Li C, Zhang S, et al. 2022. Particulate organic carbon exports from the terrestrial biosphere controlled by erosion. *Catena.* 209:105815.
- Matsushita B, Yang W, Chen J, Onda Y, Qiu G. 2007. Sensitivity of the enhanced vegetation index (EVI) and normalized difference vegetation index (NDVI) to topographic effects: a case study in high-density cypress forest. *Sensors (Basel).* 7(11):2636–2651.
- Montgomery DR. 2007. Soil erosion and agricultural sustainability. *Proc Natl Acad Sci USA.* 104(33):13268–13272.
- Panagos P, Borrelli P, Meusburger K, Yu B, Klik A, Lim KJ, Yang JE, Ni JR, Miao CY, Chattopadhyay N, et al. 2017. Global rainfall erosivity assessment based on high-temporal resolution rainfall records. *Sci Rep.* 7(1):4175.
- Peel MC, Finlayson BL, McMahon TA. 2007. Updated world map of the Köppen-Geiger climate classification. *Hydrol Earth Syst Sci.* 11(3):259–263.
- Piao SL, Friedlingstein P, Ciais P, Viovy N, Demarty J. 2007. Growing season extension and its impact on terrestrial carbon cycle in the Northern Hemisphere over the past 2 decades. *Glob Biogeochem Cycles.* 21(3).
- Pimentel D, Harvey C, Resosudarmo P, Sinclair K, Kurz D, McNair M, Crist S, Shpritz L, Fitton L, Saffouri R, et al. 1995. Environmental and economic costs of soil erosion and conservation benefits. *Science.* 267(5201):1117–1123.
- Pimentel D, Kounang N. 1998. Ecology of soil erosion in ecosystems. *Ecosystems.* 1(5):416–426.
- Pizarro R, Araya S, Jordán C, Fariás C. 2000. Peaks flows and the effects of changes in vegetation cover in the Purapel watershed, Chile. *J Hydrol.* 27:249–257.

- Poulter B, MacBean N, Hartley A, Khlystova I, Arino O, Betts R, Bontemps S, Boettcher M, Brockmann C, Defourny P, et al. 2015. Plant functional type classification for earth system models: results from the European Space Agency's Land Cover Climate Change Initiative. *Geosci Model Dev.* 8(7):2315–2328.
- Ran C, Wang SJ, Bai XY, Tan Q, Wu LH, Luo XL, Chen H, Xi HP, Lu Q. 2020. Evaluation of temporal and spatial changes of global ecosystem health. *Land Degrad Dev.* 1–13.
- Robinson DA, Panagos P, Borrelli P, Jones A, Montanarella L, Tye A, Obst CG. 2017. Soil natural capital in Europe; a framework for state and change assessment. *Sci Rep.* 7(1):6706.
- Saco PM, Moreno-de las Heras M. 2013. Ecogeomorphic coevolution of semiarid hillslopes: emergence of banded and striped vegetation patterns through interaction of biotic and abiotic processes. *Water Resour Res.* 49(1):115–126.
- Sen KP. 1968. Estimates of the Regression Coefficient Based on Kendall's Tau. *Publ Am Stat Assoc.* 63(324):1379–1389.
- Schlaepfer DR, Bradford JB, Lauenroth WK, Munson SM, Tietjen B, Hall SA, Wilson SD, Duniway MC, Jia G, Pyke DA, et al. 2017. Climate change reduces extent of temperate drylands and intensifies drought in deep soils. *Nat Commun.* 8(1):1–9.
- Shen X, An R, Quaye-Ballard JA, Zhang L, Wang Z. 2016. Evaluation of the European space agency climate change initiative soil moisture product over China using variance reduction factor. *J Am Water Resour Assoc.* 52(6):1524–1535.
- Shiono T, Ogawa S, Miyamoto T, Kameyama K. 2013. Expected impacts of climate change on rainfall erosivity of farmlands in Japan. *Ecol Eng.* 61: :678–689.
- Slayback DA, Pinzon JE, Los SO, Tucker CJ. 2003. Northern hemisphere photosynthetic trends 1982–99. *Glob Change Biol.* 9(1):1–15.
- Song X, Song S, Sun W, Mu X, Wang S, Li J, Li Y. 2015. Recent changes in extreme precipitation and drought over the Songhua River Basin, China, during 1960–2013. *Atmos Res.* 157:137–152.
- Srivastava A, Yetemen O, Saco PM, Rodriguez JF, Kumari N, Chun KP. 2022. Influence of orographic precipitation on coevolving landforms and vegetation in semi-arid ecosystems. *Earth Surf Processes Landf.* 47(12):2846–2862.
- Teng HF, Viscarra Rossel RA, Shi Z, Behrens T, Chappell A, Bui E. 2016. Assimilating satellite imagery and visible–near infrared spectroscopy to model and map soil loss by water erosion in Australia. *Environ Model Softw.* 77:156–167.
- Tian Y, Liang M, Hu B. 2015. Temporal-spatial dynamic change characteristics of evapotranspiration in Beibu Gulf Coastal Zone during 2000–2013. *Trans Chin Soc Agric Mach.* 46(8):146–158.
- Tong X, Brandt M, Yue Y, Horion S, Wang K, Keersmaecker WD, Tian F, Schurgers G, Xiao X, Luo Y, et al. 2018. Increased vegetation growth and carbon stock in China karst via ecological engineering. *Nat Sustain.* 1(1):44–50.
- Tozer B, Sandwell DT, Smith WHF, Olson C, Beale JR, Wessel P. 2019. Global bathymetry and topography at 15 arc seconds: SRTM15+. *Earth Space Sci.* 6(10):1847–1864.
- Van der Knijff JMF, Jones RJA, Montanarella L. 1999. Soil erosion risk assessment in Italy. Brussels, Belgium: European Soil Bureau, European Commission; p. 54.
- Van Oost K, Quine TA, Govers G, De Gryze S, Six J, Harden JW, Ritchie JC, McCarty GW, Heckrath G, Kosmas C, et al. 2007. The impact of agricultural soil erosion on the global carbon cycle. *Science.* 318(5850):626–629.
- Wang T. 2018. Impact of precipitation and vegetation change on soil erosion in Luohe River Basin of northern Shaanxi Province. *Jiangsu Agric Sci.* 46(20):295–300.
- Wang YX, Fang NF, Tong LS, Shi ZH. 2017. Source identification and budget evaluation of eroded organic carbon in an intensive agricultural catchment. *Agric Ecosyst Environ.* 247:290–297.
- Wen D. 1998. Agriculture in China: water and energy resources. *Agric China: 1949–2030*:479–497.
- Williams JR. 1990. The Erosion-Productivity Impact Calculator (EPIC) Model: A case history. *Philos Trans B.* 329(1255):421–428.
- Wischmeier WH, Smith DD. 1958. Rainfall energy and its relationship to soil loss. *Trans Am Geophys Union.* 39:285–291.
- Wu LH, Wang SJ, Bai XY, Tian YC, Luo GJ, Wang JF, Li Q, Chen F, Deng YH, Yang YJ, et al. 2020. Climate change weakens the positive effect of human activities on karst vegetation productivity restoration in southern China. *Ecol Indic.* 115:106392.
- Wu GL, Liu YF, Cui Z, Liu Y, Shi ZH, Yin R, Kardol P. 2020. Trade-off between vegetation type, soil erosion control and surface water in global semi-arid regions: a meta-analysis. *J Appl Ecol.* 57(5):875–885.
- Wuepper D, Borrelli P, Finger R. 2020. Countries and the global rate of soil erosion. *Nat Sustain.* 3(1): 51–55.

- Xiao B, Bai X, Zhao C, Tan Q, Li Y, Luo G, et al. 2022. Responses of carbon and water use efficiencies to climate and land use changes in China's karst areas. *J Hydrol.* 617:128968.
- Xu YQ, Shao XM. 2006. Estimation of soil erosion supported by GIS and RUSLE: a case study of Maotiaohe Watershed, Guizhou Province. *J Beijing For Univ.* 28(4):67–71.
- Yang D, Shinjiro K, Taikan O, Toshio K, Katumi M. 2003. Global potential soil erosion with reference to land use and climate changes. *Hydrol Process.* 17(14):2913–2928.
- Yang Y, Wang S, Bai X, Tan Q, Li Q, Wu L, Tian S, Hu Z, Li C, Deng Y, et al. 2019. Factors affecting long-term trends in global NDVI. *Forests.* 10(5):372.
- Zhang S, Bai X, Zhao C, Tan Q, Luo G, Wu L, Xi H, Li C, Chen F, Ran C, et al. 2022. China's carbon budget inventory from 1997 to 2017 and its challenges to achieving carbon neutral strategies. *J Cleaner Prod.* 347:130966.
- Zhu Z, Piao S, Myneni RB, Huang M, Zeng Z, Canadell JG, Ciais P, Sitch S, Friedlingstein P, Arneeth A, et al. 2016. Greening of the Earth and its drivers. *Nat Clim Change* 6(8):791–795.